Article

Current Biology

Topographic Cortico-cerebellar Networks Revealed by Visual Attention and Working Memory

Highlights

- Cerebellar lobule VIIb/VIIIa functional organization mirrors that in parietal cortex
- Dorsomedial lobule VIIb/VIIIa represents visual field and spatial locus of attention
- Ventrolateral lobule VIIb/VIIIa is recruited by visual working memory load
- Functional connectivity reveals fine-scale topography of cortico-cerebellar networks

Authors

James A. Brissenden, Sean M. Tobyne, David E. Osher, Emily J. Levin, Mark A. Halko, David C. Somers

Correspondence

somers@bu.edu

In Brief

Brissenden et al. demonstrate precise cerebellar contributions to visual cognitive processing and establish the existence of two cortico-cerebellar subnetworks that support different aspects of visuospatial cognition. This topographic specificity suggests that fine-grained cortico-cerebellar loops play a prominent role in cognitive processing.

Brissenden et al., 2018, Current Biology *28*, 3364–3372
November 5, 2018
https://doi.org/10.1016/j.cub.2018.08.059

CellPress

CellPress

Current Biology
Article

Topographic Cortico-cerebellar Networks Revealed by Visual Attention and Working Memory

James A. Brissenden,[1] Sean M. Tobyne,[1] David E. Osher,[2] Emily J. Levin,[3] Mark A. Halko,[4] and David C. Somers[1,5,*]
[1]Department of Psychological and Brain Sciences, Boston University, 64 Cummington Mall, Boston, MA 02215, USA
[2]Department of Psychology, Ohio State University, 1835 Neil Avenue, Columbus, OH 43210, USA
[3]Department of Cognitive, Linguistic, and Psychological Sciences, Brown University, 190 Thayer Street, Providence, RI 02912, USA
[4]Berenson-Allen Center for Noninvasive Brain Stimulation, Beth Israel Deaconess Medical Center, 330 Brookline Avenue, Boston, MA 02215, USA
[5]Lead Contact
*Correspondence: somers@bu.edu
https://doi.org/10.1016/j.cub.2018.08.059

SUMMARY

Substantial portions of the cerebellum appear to support non-motor functions; however, previous investigations of cerebellar involvement in cognition have revealed only a coarse degree of specificity. Although somatotopic maps have been observed within cerebellum, similar precision within cortico-cerebellar networks supporting non-motor functions has not previously been reported. Here, we find that human cerebellar lobule VIIb/VIIIa differentially codes key aspects of visuospatial cognition. Ipsilateral visuospatial representations were observed during both a visual working memory and an attentionally demanding visual receptive field-mapping fMRI task paradigm. Moreover, within lobule VIIb/VIIIa, we observed a functional dissociation between spatial coding and visual working memory processing. Visuospatial representations were found in the dorsomedial portion of lobule VIIb/VIIIa, and load-dependent visual working memory processing was shifted ventrolaterally. A similar functional gradient for spatial versus load processing was found in posterior parietal cortex. This cerebral cortical organization was well predicted by functional connectivity with spatial and load regions of cerebellar lobule VIIb/VIIIa. Collectively, our findings indicate that recruitment by visuospatial attentional functions within cerebellar lobule VIIb/VIIIa is highly specific. Furthermore, the topographic arrangement of these functions is mirrored in frontal and parietal cortex. These findings motivate a closer examination of cortico-cerebellar functional specialization across a broad range of cognitive domains.

INTRODUCTION

Dating back to the seminal work of Brodmann, a substantial body of research has sought to parcellate the cerebral cortex on the basis of cytoarchitecture, connectivity, and function (e.g., [1–3]). This work has led to the conclusion that the cerebral cortex comprises a large number of functionally specialized areas. The cerebellum, on the other hand, has traditionally been viewed as functionally homogeneous. For much of the last century, the cerebellum was primarily thought to contribute to motor control and coordination [4–6]. In recent years, functional neuroimaging has revealed evidence linking the cerebellum to cognitive functions, including attention and working memory [7–11]. Working memory, language, executive function, and affective tasks have been shown to elicit non-overlapping patterns of activation within cerebellar cortex [9, 12, 13]. Additionally, neuroanatomical tracing in primates [14] and functional connectivity analyses in humans [10, 15] indicate that regions of cerebral association cortex communicate with specific, non-motor portions of the cerebellum. Despite the exquisitely regular local circuit organization of the cerebellum, the topography of polysynaptic connections with association areas of cerebral cortex has evaded accurate description. Current evidence suggests that the cerebellum possesses a coarse functional organization that does not mirror the fine-scale specificity observed in cerebral cortex.

Here, we perform detailed investigations of closely related aspects of visuospatial attention. The current work extends prior human cerebellar research [7–10] in performing a more detailed functional mapping of the topographic organization of visuospatial attention and working memory function within the cerebellum. We observe that the dorsomedial portion of cerebellar lobule VIIb/VIIIa represents working memory targets in the ipsilateral visual field. Using population receptive field mapping, we confirm that this portion of cerebellum represents the ipsilateral visual field. Although somatotopic representations are well documented within the cerebellum, the finding of cerebellar visuospatial representations is novel. A closer examination reveals that working memory load processes recruit an overlapping but more ventrolaterally positioned portion of lobule VIIb/VIIIa. Similarly, within the cerebral cortex's dorsal attention network, we observe overlapping but dissociable patterns of activation for spatial coding and for working memory load. Remarkably, these differential patterns of visual attentional functional recruitment within the cerebral cortex are strongly predicted by functional connectivity with visuospatial and working memory load processing domains in cerebellar lobule VIIb/VIIIa. These findings reveal a high degree of specificity in the functional organization of the cerebellum and cortico-cerebellar circuitry.

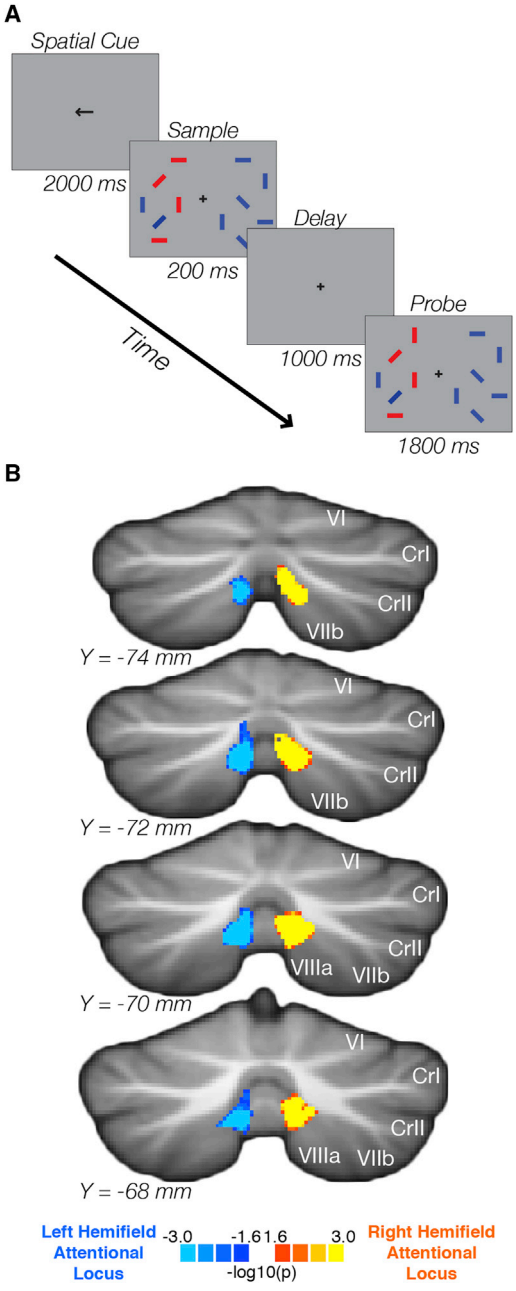

Figure 1. Visuospatial Working Memory

(A) Task configuration. Participants held central fixation while covertly performing a spatially lateralized visual working memory task, in which they were asked to encode the orientation of 1 or 4 target stimuli (red) and to report whether the orientation of any bar changed (one bar changed on 50% of trials; no change on other 50% of trials) across a brief delay interval. Target stimuli alternated visual hemifields across blocks of trials.

(B) Cerebellar spatial classification discriminance group map (n = 9) produced by a multivariate feature weight mapping analysis (FWM). Hot or cool colors indicate voxels or features that influenced the classification decision toward the right or left hemifield attentional locus, respectively. Map is thresholded at $p < 0.05$ FWE corrected, two-sided. CrI, Crus I; CrII, Crus II; VI, lobule VI; VIIb, lobule VIIb; VIIIa, lobule VIIIa.

RESULTS

To investigate spatial coding of visual attention within the cerebellum, we asked participants (n = 9) to perform a lateralized visual working memory task in an fMRI scanner (Figure 1A). At the beginning of each block, participants were cued to covertly attend either the left or right visual hemifield while holding central fixation. Participants were instructed to maintain in working memory the orientation of briefly presented (200 ms) target items (red bars) in the attended hemifield over short delays. Visual working memory (VWM) load also was varied by presenting 1 or 4 targets in different blocks (results presented in Figure 3). Distractor stimuli (blue bars) were included to equate visual stimulation between attended and unattended hemifields. The locus of attention (left versus right) did not influence behavioral measures of accuracy (d'; $t(8) = 0.0066$; $p = 0.995$) or reaction time ($t(8) = 0.0017$; $p = 0.999$). We observed that the location of covert attentional deployment (left or right visual hemifield) could be decoded from whole cerebellum multi-voxel blood-oxygen-level-dependent (BOLD) activity patterns. Mean classification accuracy was 60.42% (±1.54% SEM) relative to chance performance of 50%. Non-parametric permutation tests showed that the mean classification accuracy produced by the whole-cerebellum region of interest (ROI) fell outside the bounds of the 95% confidence interval of the generated null distribution ($p = 0.001$).

Visuospatial Selectivity within Cerebellar Lobule VIIb/VIIIa

To localize the cerebellar regions that exhibit attentional spatial sensitivity, we performed a multivariate feature weight mapping (FWM) analysis on whole-cerebellum BOLD activity patterns (see STAR Methods for details). Submitting individual subject feature weight discriminance maps to a 2nd-level group analysis revealed clusters of discriminative voxels in both left and right cerebellar lobule VIIb/VIIIa (Figure 1B; MNI152/SUIT coordinates: [−6.5, −70.2, −42.5]; [9.0, −71.1, −41.4]). The clusters of significant feature or voxel weights in each hemisphere were oppositely signed, indicating that these clusters influenced the classification decision toward different classes (i.e., hemifields). The cluster in left lobule VIIb/VIIIa was found to weight the decision function toward the left hemifield attentional locus, and the cluster in right lobule VIIb/VIIIa was found to weight the decision function toward the right hemifield attentional locus. Thus, these cerebellar responses code for attentional processing within the ipsilateral visual hemifield, and cerebral cortical regions encode contralateral visual field representations [16]. This relationship is consistent with the hemispheric crossing of polysynaptic neuronal pathways connecting cerebral cortex and cerebellum; the cortico-ponto-cerebellar and cerebello-thalamo-cortical fiber tracts each cross the midline via the decussation of the middle and superior cerebellar peduncle, respectively. Cerebral cortical sensitivity to the locus of spatial attention estimated by FWM is shown in Figure S1. Cortical spatial sensitivity was found to be largely restricted to extrastriate cortex and the intraparietal sulcus (IPS), consistent with prior observations [16–20].

Eye Movement Control

The cerebellum has been implicated in oculomotor control, and some have argued that cerebellar attentional activation reflects

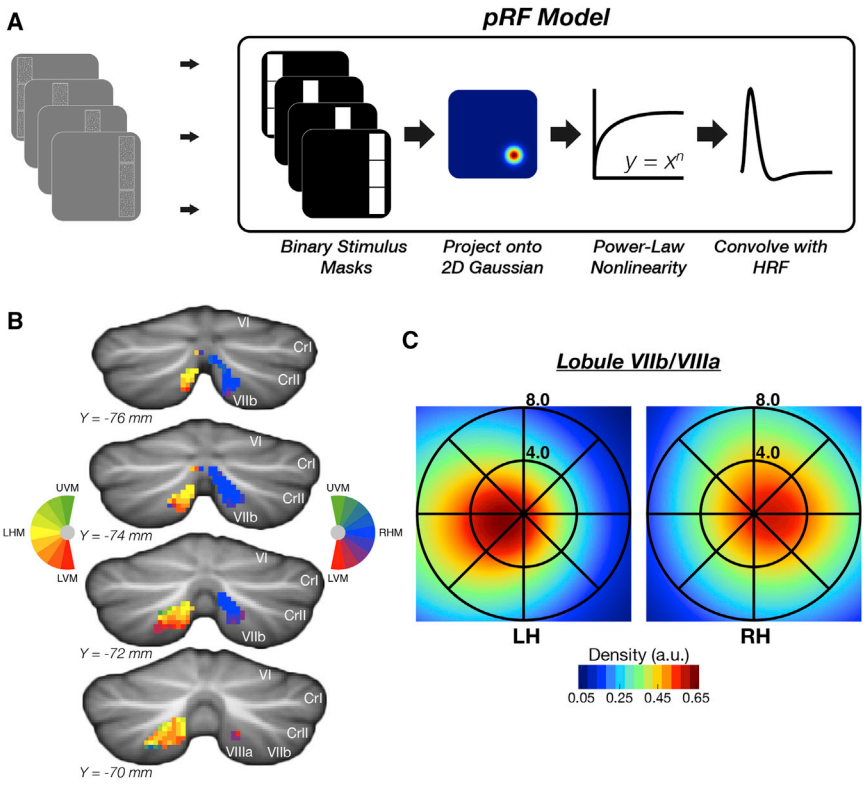

Figure 2. Visual Stimulation and Visual Attention

(A) Participants held central fixation while bar-like apertures containing moving dot stimuli were slowly swept across the visual field in each of four cardinal directions. The task was to report which of the two outer sections possessed dot motion in the same direction as the inner section. This task was repeated for each step in the visual field sweep. fMRI responses were used to estimate the population receptive field for each ventral cerebellar voxel.

(B) Polar angle visual field mapping in ventral cerebellum of one participant revealed ipsilateral visual field representations within the dorsomedial portion of cerebellar lobule VIIb/VIIIa.

(C) Group-average (n = 5) visual field coverage maps for cerebellar lobule VIIb/VIIIa also revealed coding of ipsilateral visual space. Note that X and Y axes represent visual field position, and the color map reflects the density of visual field coverage. See also Figure S4.

oculomotor behavior rather than true involvement in attention (e.g., [21]). Therefore, it is critical to examine whether our finding of visuospatial sensitivity in the cerebellum simply reflects eye-movement-related processing. All subjects possessed extensive experience at performing psychophysical tasks while maintaining fixation on a central crosshair. In-scanner eye tracking confirmed that subjects tightly held central fixation through all conditions; there was no significant difference between attend-left and attend-right trials in root-mean-square (RMS) deviation from fixation ($t(7) = 0.84$; $p = 0.43$) or horizontal eye position ($t(7) = 1.54$; $p = 0.17$). To further examine oculomotor factors as a possible source of cerebellar spatial selectivity, we investigated whether cerebellar BOLD signal predicted eye movements or eye position. We employed a support vector regression model trained on the cerebellar voxels identified as spatially discriminative by the multivariate feature weight mapping analysis (see STAR Methods). Model performance was assessed by computing a cross-validated coefficient of determination (see STAR Methods). Predictions yielded a negative coefficient of determination for both RMS deviation and average horizontal gaze position, indicating that both models performed no better than a null model in which the response of each test set observation was predicted to be the mean response of the training set (RMS deviation $R^2_{cv} = -1.65 \pm 0.42$ SEM; X coordinate $R^2_{cv} = -1.48 \pm 0.55$ SEM). Therefore, we find that cerebellar BOLD signal was not predictive of eye movements or position.

Cerebellar Visual Field Representations

As a further examination of visuospatial sensitivity in cerebellar lobule VIIb/VIIIa, we conducted a second experiment to investigate whether lobule VIIb/VIIIa contains visual field representations. The task required participants (n = 5) to covertly attend to a rectangular stimulus that moved slowly across the visual field in different directions. Thus, the entire visual field was parametrically mapped across multiple stimulus sweeps. The stimulus was divided into three segments, each containing random dot motion stimuli (see Figure 2A). On each trial, subjects were asked to report which of the two outer segments exhibited the same global motion direction as that of the inner segment. This task, which combines both spatially specific attention and visual stimulation, has previously been employed to map visual field representations in the cerebral cortex [22]. We performed population receptive field (pRF) modeling (see STAR Methods for details) on the resulting data for ventral cerebellum. Polar angle analysis revealed a representation of ipsilateral visual hemifield within dorsomedial lobule VIIb/VIIIa (Figure 2B), consistent with the findings of the hemifield classification. To reveal the representation of the visual field in lobule VIIb/VIIIa across all subjects, we computed a visual field coverage density map. This entails averaging the pRFs of above-threshold voxels ($r_{cv} > 0.2$) within an anatomical region of interest (anatomical lobule VIIb and VIIIa mask) within and across subjects. Lobule VIIb/VIIIa coverage density showed a clear bias toward ipsilateral visual hemifield locations (Figure 2C). Additionally, the extent and laterality of visual field coverage in lobule VIIb/VIIIa mirrors the visual field coverage of attention areas in fronto-parietal cortex (see Figure 6 in [22]). Lobule VIIb/VIIIa also appears to contain an over-representation of the lower visual field, similar to that observed in the visuotopic areas of intraparietal sulcus [23]; the dorsal subdivisions of early visual cortical areas V1, V2, and V3 code only the lower visual field, and a lower field bias persists throughout the dorsal visual pathway in the cerebral cortex. Experiment 2 replicates the experiment 1 finding of visuospatial selectivity within the dorsomedial portion of cerebellar lobule VIIb/VIIIa. Furthermore, these

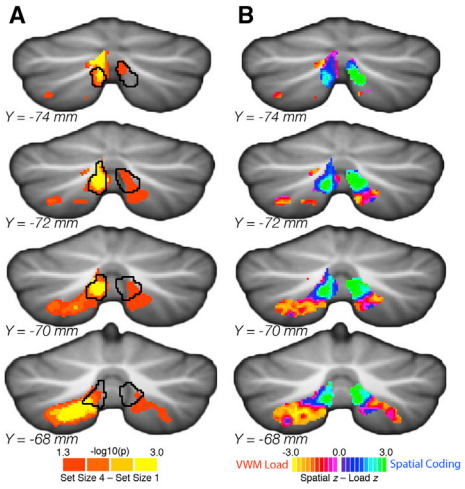

Figure 3. Visuospatial Functional Specificity within Cerebellar Lobule VIIb/VIIIa

(A) Visual working memory (VWM) load (set size 4 versus set size 1, irrespective of stimulus hemifield) drove activity broadly across cerebellar lobule VIIb/VIIIa. Black outlines indicate the extent of spatial coding from Figure 1B.

(B) Normalized comparison of spatial location coding and VWM load coding revealed complementary gradients, for which spatial coding is more robust dorsomedially and VWM load coding is more robust ventrolaterally.

(C and D) Probability density curves for VWM load coding (orange) and for spatial coding (blue) showed separable profiles in the (C) X and (D) Z dimensions (MNI coordinates).

See also Figures S2, S3, and S4.

findings critically demonstrate that cerebellar representations of the visual field mirror those previously reported in parietal and frontal cerebral cortices.

Visuospatial Functional Specificity within Cerebellar Lobule VIIb/VIIIa

To further examine the fine-scale functional organization of visuospatial attention processing within cerebellar lobule VIIb/VIIIa, we compared the locus of visuospatial selectivity with the locus of sensitivity to visual working memory load within ventral cerebellum. The visual working memory experiment (see Figure 1A; STAR Methods) [10] manipulated the number of items held in VWM (VWM load) and the hemifield of the targets while keeping stimulus drive equivalent across conditions. Overlapping but different regions were found to be sensitive to visuospatial location and to VWM load. VWM load activation extended much farther ventrolaterally within lobule VIIb/VIIIa than did the spatial sensitivity (Figure 3A). Working memory load has also been shown to activate additional areas located in dorsal cerebellum (lobule VI and Crus I) [8, 10]. However, as we did not observe spatial selectivity in dorsal cerebellum, subsequent analyses comparing VWM load and spatial coding were restricted to ventral cerebellum (dorsal cerebellum is masked in Figures 3A and 3B). Cerebral cortical sensitivity to VWM load is shown in Figure S1. To more closely examine the degree of specificity for spatial coding and VWM coding within lobule VIIb/VIIIa, we normalized the uncorrected group statistic map of each analysis across cerebellar lobule VIIb/VIIIa and then contrasted (via subtraction) the normalized spatial coding map with the normalized VWM load map. The resulting difference map was masked to exclude voxels that did not survive multiple comparison correction in both analyses. This analysis revealed a functional gradient for visuospatial attention running from dorsomedial to ventrolateral across lobule VIIb/VIIIa (Figures 3B and S2).

In order to better characterize the anatomical distinctions within lobule VIIb/VIIIa between spatial coding and VWM load coding, we constructed probability density functions of the spatial-dominant (spatial > load) and of the load-dominant (load > spatial) voxels for each of the X, Y, and Z Montreal Neurological Institute (MNI) anatomical axes (see Figures 3C, 3D, and S3). The distinction between these two populations is very clear across both the X (mediolateral) and Z (dorsoventral) axes. Spatial coding more strongly recruits the dorsomedial portion of lobule VIIb/VIIIa bilaterally, and VWM load more strongly recruits the ventrolateral portion of lobule VIIb/VIIIa bilaterally.

Within dorsomedial lobule VIIb/VIIIa, many voxels exhibited both significant spatial coding and significant load coding (Figures 3A and 3B). To examine the relationship between visual field representations and space versus load coding, we constructed separate visual field coverage density maps weighted by load effect size and by spatial effect size. This analysis, which was limited to the subjects who participated in both studies (n = 3), used all voxels with significant visual pRF fits ($r_{cv} > 0.2$). The weighted visual field representations closely matched each other and the unweighted representation (Figure S4), although in the right hemisphere, spatial coding emphasized the peripheral ipsilateral visual field more so than did load coding.

Topographically Organized Cortico-cerebellar Networks

The fine-scale functional organization within cerebellar lobule VIIb/VIIIa mirrored the organization observed in the cerebral cortex. Spatial selectivity was stronger within extrastriate cortex and along the medial bank of intraparietal sulcus, which dovetails with previous work identifying retinotopic maps within these areas [16, 22, 23]. VWM load activation, on the other hand, dominated in the more anterior and ventral portions of the intraparietal sulcus (Figure 4A).

The observation of similar functional gradients in cerebellar lobule VIIb/VIIIa and parieto-occipital cortex raises the question of whether highly specific functional subnetworks for visuospatial attention processing exist between cerebellum and the cerebral cortex. To address this question, we examined whether resting-state functional connectivity with cerebellar lobule VIIb/VIIIa could predict the functional organization in parieto-occipital cortex. Spatial coding seed and VWM load seed ROIs in lobule VIIb/VIIIa were defined in each hemisphere using the multiple comparison corrected group map from each analysis. These ROIs included any lobule VIIb/VIIIa voxel that survived correction

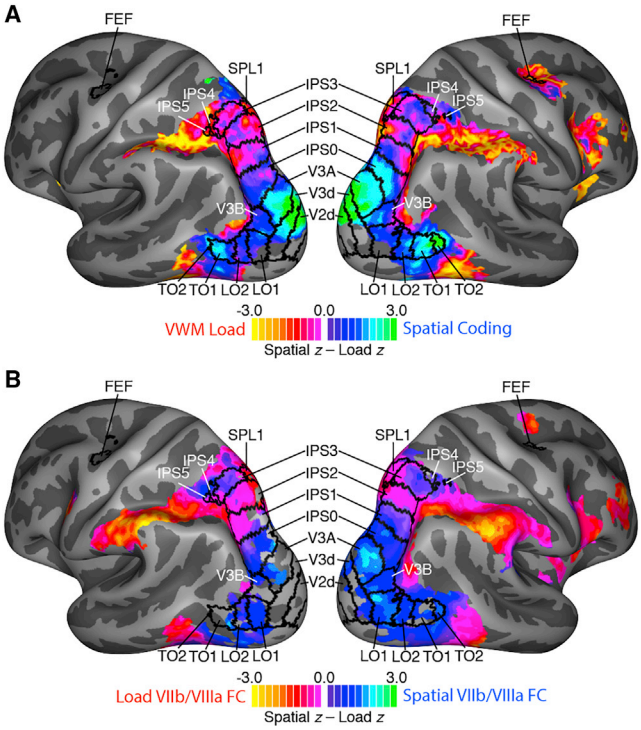

Figure 4. Specificity of Cortico-cerebellar Subnetworks

(A) Normalized comparison of spatial coding and VWM load coding in the cerebral cortex revealed a gradient in parieto-occipital cortical regions. Areal boundaries from a probabilistic retinotopy atlas [23] are overlaid. Within parietal cortex, dorsomedial retinotopic areas IPS0, IPS1, IPS2, IPS3, IPS4, and IPS5 exhibited varying degrees of spatial bias, and the ventrolateral portion of IPS was biased for VWM load coding.

(B) Contrast between resting-state functional connectivity of cerebellar lobule VIIb/VIIIa spatial coding and VWM load coding seeds accurately reflected the functional gradient observed in the task data of (A).

See also Figure S1.

for multiple comparisons in each respective analysis (load: $p < 0.05$ FWE corrected, one-sided; spatial: $p < 0.05$ FWE corrected, two-sided; Figures 1A and 3B). No constraints were placed on the overlap between load and spatial coding ROIs. For each cerebellar ROI, we extracted average resting-state time courses and then computed their correlations with the resting-state time course from each vertex from the contralateral hemisphere of cerebral cortex, using data from 14 subjects (see STAR Methods). A difference analysis of spatial and load seed connectivity yielded a prediction of parieto-occipital functional organization (Figure 4B). Spatially selective cerebellar voxels exhibited stronger functional connectivity with extrastriate cortex and the medial bank of IPS, and load-activated cerebellar voxels exhibited stronger functional connectivity with anterior IPS and frontal areas. This functional gradient, produced from resting-state functional connectivity, closely matches the actual functional gradient observed in the task data (Figure 4A). Spatially correlating the connectivity difference map with the task recruitment difference map yielded very strong correlations for each hemisphere (right hemisphere [RH]: $r = 0.84$, $p < 0.000001$; left hemisphere [LH]: $r = 0.70$, $p < 0.000001$). These results provide evidence for fine-grained functional subnetworks for visual attention and working memory spanning both cerebellar lobule VIIb/VIIIa and parieto-occipital cortex.

DISCUSSION

These findings reveal a highly specific functional organization for visuospatial attention and working memory within cerebellar lobule VIIb/VIIIa. Here, for the first time, we demonstrate that the cerebellum encodes representations of the visual field. Spatially selective responses were found in cerebellar lobule VIIb/VIIIa across two independent tasks that required allocating attention to different portions of the visual display. Additionally, a functional gradient for visuospatial attention processing was observed running from dorsomedial to ventrolateral within lobule VIIb/VIIIa. The dorsomedial portion of lobule VIIb/VIIIa was more strongly recruited by spatial aspects of the task, and ventrolateral lobule VIIb/VIIIa was more strongly recruited by increases in VWM load. The observed functional specificity in lobule VIIb/VIIIa was reflected in the connectivity of these areas with cerebral cortex. Seed-based intrinsic functional connectivity analyses showed that cortico-cerebellar connectivity of load- and space-sensitive portions of cerebellar lobule VIIb/VIIIa precisely predicted the specialization observed in cortex. Taken together, these findings indicate the existence of fine-scale cortico-cerebellar networks that differentially encode key functional aspects of visual attentional processing.

Our findings extend prior work demonstrating the specificity of cortico-cerebellar connections. Anatomical tracer studies performed in non-human primates have shown that cerebellar regions project to the same cerebral cortical regions from which they receive input forming closed-loop circuits [14]. Additionally, cortico-cerebellar circuits connecting cerebellum with pre-frontal cortex area 46 are shown to be distinct from circuits connecting cerebellum with M1 [14]. There is also evidence for anatomical projections from cerebellar output nuclei to specific portions of posterior parietal cortex [24]. Work in humans using resting-state fMRI provides complementary evidence for extensive cortico-cerebellar projections that can be segregated into motor and cognitive domains [15, 25, 26].

Due to the uniformity of cerebellar cytoarchitecture, it has been suggested that differences in information processing across cerebellar cortex arise from differences in connectivity [27]. Indeed, cerebellar intrinsic coupling with foot, hand, and tongue areas of primary motor cortex precisely predicts task-based estimates of cerebellar somatomotor topography [15]. We previously showed that cortico-cerebellar resting-state functional connectivity can also predict cerebellar recruitment by cognitive tasks. Cerebellar functional connectivity with fronto-parietal cortex was found to be strongly associated with the magnitude of cerebellar activation by working memory and attention [10]. In the current study, we showed that two regions within cerebellar lobule VIIb/VIIIa exhibited differential connectivity patterns with cerebral cortex and that these differences precisely mirrored the specialization observed in parieto-occipital cortex.

It should be noted that we cannot definitively attribute our set size effect to VWM storage processes. The VWM change detection task used here employed a block design. Consequently, the load contrast could potentially reveal differences during

selection, encoding, maintenance periods, and/or probe periods of a trial; future studies will be needed to isolate which VWM task components specifically contribute to the observed load effects.

Cerebellar somatomotor representations have been extensively mapped in both non-humans and humans [15, 28–32]. The cerebellum contains two full-body maps. An inverted map is found in lobules IV and V within the anterior lobe, and a second upright map is found in lobule VIIIb within the posterior lobe [15, 31]. No prior work has investigated whether non-motor topographic representations exist within the portion of the cerebellum intervening these areas. Here, we find strong evidence for an ipsilateral visual hemifield representation within lobule VIIb/VIIIa, mirroring the ipsilateral representation of the body within the two cerebellar somatomotor maps. Future work will need to determine whether a more fine-grained topographic organization exists within these hemifield representations. It is possible that cerebellar lobule VIIb/VIIIa may contain fine-scale representations of within-hemifield locations but may not be retinotopically organized. Physiological studies have shown that nearby areas of somatotopic cerebellar cortex respond to stimulation of distinct portions of a particular body part. This disordered representation has been referred to as ''fractured somatotopy'' [33–35]. Nevertheless, local voxel patterns in both cerebellar motor maps have been shown to discriminate the stimulation or movement of individual fingers, indicating the existence of finger representations in these areas [32]. Consequently, fine-scale representations of within-hemifield locations may exist in dorsomedial lobule VIIb/VIIIa, even in the absence of an orderly organization.

Prior work has reported that verbal working memory recruits cerebellar lobule VII [8]. The combination of the present and prior findings suggests that lobule VII may support generalized working memory functions. Alternatively, modality-specific subdomains of lobule VII could exist to support different forms of working memory, similar to recent observations in lateral frontal cortex [36]. A broad range of cerebellar contributions to visual perception have been observed (e.g., [37]). Patients with lesions to lobule VIIb/VIIIa (and to Crus I and Crus II) exhibit covert attention deficits [38], and lesions to left hemisphere lobule VIIb/VIIIa have been associated with deficits in visual processing of biological motion [39], consistent with a functional role in dorsal attention network processing. Increasing evidence points to an association between reduced cerebellar gray matter volume, particularly within cerebellar lobule VIIb, and psychiatric disease [40, 41]. These studies are largely consistent with our finding of attentional organization within lobule VIIb/VIIIa. However, the relationship between cerebellar measures and clinical symptom severity has not been examined at the level of granularity of within-system organization we report here.

Within posterior parietal cortex, dorsomedial portions of the IPS contain robust visual field representations [16, 22, 23] and are also activated by VWM load [42–44], and the adjacent ventral and lateral portions of IPS exhibit VWM load dependence but do not possess clear visual field representations. Similarly, within cerebellar lobule VIIb/VIIIa, we observed that the dorsomedial portion contains robust visual field representations and is activated by VWM load, and the ventrolateral portion is strongly recruited by VWM load but lacks clear visual field representations. Further research is needed to differentiate the functional contributions of dorsomedial and ventrolateral portions of cerebellar lobule VIIb/VIIIa from those of their cerebral cortical counterparts. The uniformity of cerebellar cytoarchitecture has led to proposals that cerebellar computations are similarly uniform [27, 45]. One prominent theory, paralleling well-established ideas concerning the role of the cerebellum in motor learning [5, 46–49], proposes that cerebellar regions form internal models that coordinate and refine cognitive operations [11, 50]. In the motor domain, cerebellar internal models are conceptualized as predicting the sensory consequences of a motor action (forward model) or as generating the motor commands necessary to achieve a desired state or goal (inverse model) [48, 50]. Ultimately, the hypothesized purpose of these models is to enable the efficient coordination of motor actions necessary for skilled behavior. Consequently, the cerebellum may play a similar role in attentional processing, serving to refine the precise spatiotemporal deployment of visuospatial attention in familiar contexts.

These findings not only have implications for our understanding of how the brain's circuitry precisely controls the deployment of limited visual attentional resources but also provide evidence for the existence of highly specific cortico-cerebellar functional networks for cognitive processing. We hypothesize that similarly precise cortico-cerebellar networks exist for many other aspects of cognition and that the observed functional and connective specificity may reflect a general governing principle of cortico-cerebellar topographic organization. In order to observe such networks, it may prove useful to follow the methodological approach that was employed here by combining high-resolution functional connectivity analysis with multiple task-based fMRI paradigms that target closely related cognitive processes.

STAR★METHODS

Detailed methods are provided in the online version of this paper and include the following:

- KEY RESOURCES TABLE
- CONTACT FOR REAGENT AND RESOURCE SHARING
- EXPERIMENTAL MODEL AND SUBJECT DETAILS
- METHOD DETAILS
  - Magnetic Resonance Image Acquisition
  - Magnetic Resonance Image Preprocessing
  - Visual stimuli and experimental paradigm
- QUANTIFICATION AND STATISTICAL ANALYSIS
  - Multivariate pattern analysis
  - Multivariate feature weight mapping
  - Eye movement control analysis
  - VWM load/spatial coding selectivity analysis
  - Population receptive field modeling
- DATA AND SOFTWARE AVAILABILITY

SUPPLEMENTAL INFORMATION

Supplemental Information includes four figures and can be found with this article online at https://doi.org/10.1016/j.cub.2018.08.059.

ACKNOWLEDGMENTS

We thank Thomas Benner and Himanshu Bhat of Siemens Medical Solutions, Steven Cauley of Massachusetts General Hospital, and the University of Minnesota Center for Magnetic Resonance Research for modifying and for

supplying the simultaneous multi-slice-BOLD imaging sequences used in this work; Kathryn Devaney and Maya Rosen for assistance with data collection; Yi Chen and Johannes Stelzer for advice on statistical methods; and Sam Ling for helpful comments on the manuscript. This work was supported by the NIH (NIH R01EY022229 and NIH R21EY027703 to D.C.S. and R01MH111868 to M.A.H.), National Science Foundation (NSF Graduate Research Fellowship DGE-1247312 to J.A.B.), and Sidney R. Baer, Jr. Foundation (M.A.H.).

AUTHOR CONTRIBUTIONS

J.A.B., M.A.H., and D.C.S. designed the study. J.A.B., S.M.T., and E.J.L. collected the data. J.A.B., S.M.T., D.E.O., and D.C.S. analyzed the data. J.A.B., M.A.H., and D.C.S. drafted the paper.

DECLARATION OF INTERESTS

The authors declare no competing interests.

Received: June 18, 2018
Revised: August 3, 2018
Accepted: August 29, 2018
Published: October 18, 2018

REFERENCES

1. Brodmann, K. (1909). Vergleichende Lokalisationslehre der Grosshirnrinde in ihren Prinzipien dargestellt aufgrund des Zellenbaues (Leipzig: Barth).
2. Yeo, B.T.T., Krienen, F.M., Sepulcre, J., Sabuncu, M.R., Lashkari, D., Hollinshead, M., Roffman, J.L., Smoller, J.W., Zöllei, L., Polimeni, J.R., et al. (2011). The organization of the human cerebral cortex estimated by intrinsic functional connectivity. J. Neurophysiol. *106*, 1125–1165.
3. Glasser, M.F., Coalson, T.S., Robinson, E.C., Hacker, C.D., Harwell, J., Yacoub, E., Ugurbil, K., Andersson, J., Beckmann, C.F., Jenkinson, M., et al. (2016). A multi-modal parcellation of human cerebral cortex. Nature *536*, 171–178.
4. Evarts, E.V., and Thach, W.T. (1969). Motor mechanisms of the CNS: cerebrocerebellar interrelations. Annu. Rev. Physiol. *31*, 451–498.
5. Ito, M. (1984). The Cerebellum and Neural Control (Raven Press).
6. Llinás, R. (1984). Functional significance of the basic cerebellar circuit in motor coordination. In Cerebellar Functions. Proceedings in Life Sciences, J.R. Bloedel, J. Dichgans, and W. Precht, eds. (Berlin, Heidelberg: Springer), pp. 170–185.
7. Allen, G., Buxton, R.B., Wong, E.C., and Courchesne, E. (1997). Attentional activation of the cerebellum independent of motor involvement. Science *275*, 1940–1943.
8. Chen, S.H.A., and Desmond, J.E. (2005). Cerebrocerebellar networks during articulatory rehearsal and verbal working memory tasks. Neuroimage *24*, 332–338.
9. Stoodley, C.J., Valera, E.M., and Schmahmann, J.D. (2012). Functional topography of the cerebellum for motor and cognitive tasks: an fMRI study. Neuroimage *59*, 1560–1570.
10. Brissenden, J.A., Levin, E.J., Osher, D.E., Halko, M.A., and Somers, D.C. (2016). Functional evidence for a cerebellar node of the dorsal attention network. J. Neurosci. *36*, 6083–6096.
11. Sokolov, A.A., Miall, R.C., and Ivry, R.B. (2017). The cerebellum: adaptive prediction for movement and cognition. Trends Cogn. Sci. *21*, 313–332.
12. Stoodley, C.J., and Schmahmann, J.D. (2009). Functional topography in the human cerebellum: a meta-analysis of neuroimaging studies. Neuroimage *44*, 489–501.
13. Guell, X., Gabrieli, J.D.E., and Schmahmann, J.D. (2018). Triple representation of language, working memory, social and emotion processing in the cerebellum: convergent evidence from task and seed-based resting-state fMRI analyses in a single large cohort. Neuroimage *172*, 437–449.
14. Kelly, R.M., and Strick, P.L. (2003). Cerebellar loops with motor cortex and prefrontal cortex of a nonhuman primate. J. Neurosci. *23*, 8432–8444.
15. Buckner, R.L., Krienen, F.M., Castellanos, A., Diaz, J.C., and Yeo, B.T.T. (2011). The organization of the human cerebellum estimated by intrinsic functional connectivity. J. Neurophysiol. *106*, 2322–2345.
16. Swisher, J.D., Halko, M.A., Merabet, L.B., McMains, S.A., and Somers, D.C. (2007). Visual topography of human intraparietal sulcus. J. Neurosci. *27*, 5326–5337.
17. Serences, J.T., and Yantis, S. (2007). Spatially selective representations of voluntary and stimulus-driven attentional priority in human occipital, parietal, and frontal cortex. Cereb. Cortex *17*, 284–293.
18. Szczepanski, S.M., Konen, C.S., and Kastner, S. (2010). Mechanisms of spatial attention control in frontal and parietal cortex. J. Neurosci. *30*, 148–160.
19. Kalberlah, C., Chen, Y., Heinzle, J., and Haynes, J.-D. (2011). Beyond topographic representation: decoding visuospatial attention from local activity patterns in the human frontal cortex. Int. J. Imaging Syst. Technol. *21*, 201–210.
20. Jerde, T.A., Merriam, E.P., Riggall, A.C., Hedges, J.H., and Curtis, C.E. (2012). Prioritized maps of space in human frontoparietal cortex. J. Neurosci. *32*, 17382–17390.
21. Haarmeier, T., and Thier, P. (2007). The attentive cerebellum - myth or reality? Cerebellum *6*, 177–183.
22. Mackey, W.E., Winawer, J., and Curtis, C.E. (2017). Visual field map clusters in human frontoparietal cortex. eLife *6*, 1–23.
23. Wang, L., Mruczek, R.E.B., Arcaro, M.J., and Kastner, S. (2015). Probabilistic maps of visual topography in human cortex. Cereb. Cortex *25*, 3911–3931.
24. Prevosto, V., Graf, W., and Ugolini, G. (2010). Cerebellar inputs to intraparietal cortex areas LIP and MIP: functional frameworks for adaptive control of eye movements, reaching, and arm/eye/head movement coordination. Cereb. Cortex *20*, 214–228.
25. Habas, C., Kamdar, N., Nguyen, D., Prater, K., Beckmann, C.F., Menon, V., and Greicius, M.D. (2009). Distinct cerebellar contributions to intrinsic connectivity networks. J. Neurosci. *29*, 8586–8594.
26. O'Reilly, J.X., Beckmann, C.F., Tomassini, V., Ramnani, N., and Johansen-Berg, H. (2010). Distinct and overlapping functional zones in the cerebellum defined by resting state functional connectivity. Cereb. Cortex *20*, 953–965.
27. Ramnani, N. (2006). The primate cortico-cerebellar system: anatomy and function. Nat. Rev. Neurosci. *7*, 511–522.
28. Adrian, E.D. (1943). Afferent areas in the cerebellum connected with the limbs. Brain *66*, 289–315.
29. Snider, R.S., and Stowell, A. (1943). Receiving areas of the tactile, auditory, and visual systems in the cerebellum. J. Neurophysiol. *7*, 331–357.
30. Rijntjes, M., Buechel, C., Kiebel, S., and Weiller, C. (1999). Multiple somatotopic representations in the human cerebellum. Neuroreport *10*, 3653–3658.
31. Grodd, W., Hülsmann, E., Lotze, M., Wildgruber, D., and Erb, M. (2001). Sensorimotor mapping of the human cerebellum: fMRI evidence of somatotopic organization. Hum. Brain Mapp. *13*, 55–73.
32. Wiestler, T., McGonigle, D.J., and Diedrichsen, J. (2011). Integration of sensory and motor representations of single fingers in the human cerebellum. J. Neurophysiol. *105*, 3042–3053.
33. Shambes, G.M., Gibson, J.M., and Welker, W. (1978). Fractured somatotopy in granule cell tactile areas of rat cerebellar hemispheres revealed by micromapping. Brain Behav. Evol. *15*, 94–140.
34. Kassel, J., Shambes, G.M., and Welker, W. (1984). Fractured cutaneous projections to the granule cell layer of the posterior cerebellar hemisphere of the domestic cat. J. Comp. Neurol. *225*, 458–468.
35. Schlerf, J., Wiestler, T., Verstynen, T., and Diedrichsen, J. (2014). Big challenges from the little brain – imaging the cerebellum. In Advanced Brain Neuroimaging Topics in Health and Disease – Methods and Applications, T.D. Papageorgiou, G.I. Christopoulos, and S.M. Smirnakis, eds. (Rijeka: InTech), pp. 199–223.

36. Michalka, S.W., Kong, L., Rosen, M.L., Shinn-Cunningham, B.G., and Somers, D.C. (2015). Short-term memory for space and time flexibly recruit complementary sensory-biased frontal lobe attention networks. Neuron *87*, 882–892.
37. Baumann, O., Borra, R.J., Bower, J.M., Cullen, K.E., Habas, C., Ivry, R.B., Leggio, M., Mattingley, J.B., Molinari, M., Moulton, E.A., et al. (2015). Consensus paper: the role of the cerebellum in perceptual processes. Cerebellum *14*, 197–220.
38. Striemer, C.L., Cantelmi, D., Cusimano, M.D., Danckert, J.A., and Schweizer, T.A. (2015). Deficits in reflexive covert attention following cerebellar injury. Front. Hum. Neurosci. *9*, 428.
39. Sokolov, A.A., Gharabaghi, A., Tatagiba, M.S., and Pavlova, M. (2010). Cerebellar engagement in an action observation network. Cereb. Cortex *20*, 486–491.
40. Romer, A.L., Knodt, A.R., Houts, R., Brigidi, B.D., Moffitt, T.E., Caspi, A., and Hariri, A.R. (2018). Structural alterations within cerebellar circuitry are associated with general liability for common mental disorders. Mol. Psychiatry *23*, 1084–1090.
41. Moberget, T., Doan, N.T., Alnæs, D., Kaufmann, T., Córdova-Palomera, A., Lagerberg, T.V., Diedrichsen, J., Schwarz, E., Zink, M., Eisenacher, S., et al.; KaSP (2018). Cerebellar volume and cerebellocerebral structural covariance in schizophrenia: a multisite mega-analysis of 983 patients and 1349 healthy controls. Mol. Psychiatry *23*, 1512–1520.
42. Todd, J.J., and Marois, R. (2004). Capacity limit of visual short-term memory in human posterior parietal cortex. Nature *428*, 751–754.
43. Sheremata, S.L., Bettencourt, K.C., and Somers, D.C. (2010). Hemispheric asymmetry in visuotopic posterior parietal cortex emerges with visual short-term memory load. J. Neurosci. *30*, 12581–12588.
44. Sprague, T.C., Ester, E.F., and Serences, J.T. (2014). Reconstructions of information in visual spatial working memory degrade with memory load. Curr. Biol. *24*, 2174–2180.
45. Schmahmann, J.D. (1991). An emerging concept. The cerebellar contribution to higher function. Arch. Neurol. *48*, 1178–1187.
46. Marr, D. (1969). A theory of cerebellar cortex. J. Physiol. *202*, 437–470.
47. Albus, J.S. (1971). A theory of cerebellar function. Math. Biosci. *10*, 25–61.
48. Wolpert, D.M., Miall, R.C., and Kawato, M. (1998). Internal models in the cerebellum. Trends Cogn. Sci. *2*, 338–347.
49. Doya, K. (1999). What are the computations of the cerebellum, the basal ganglia and the cerebral cortex? Neural Netw. *12*, 961–974.
50. Ito, M. (2008). Control of mental activities by internal models in the cerebellum. Nat. Rev. Neurosci. *9*, 304–313.
51. Fischl, B. (2012). FreeSurfer. Neuroimage *62*, 774–781.
52. Smith, S.M., Jenkinson, M., Woolrich, M.W., Beckmann, C.F., Behrens, T.E.J., Johansen-Berg, H., Bannister, P.R., De Luca, M., Drobnjak, I., Flitney, D.E., et al. (2004). Advances in functional and structural MR image analysis and implementation as FSL. Neuroimage *23* (*Suppl 1*), S208–S219.
53. Jenkinson, M., Beckmann, C.F., Behrens, T.E.J., Woolrich, M.W., and Smith, S.M. (2012). FSL. Neuroimage *62*, 782–790.
54. Diedrichsen, J. (2006). A spatially unbiased atlas template of the human cerebellum. Neuroimage *33*, 127–138.
55. Diedrichsen, J., Balsters, J.H., Flavell, J., Cussans, E., and Ramnani, N. (2009). A probabilistic MR atlas of the human cerebellum. Neuroimage *46*, 39–46.
56. Brainard, D.H. (1997). The Psychophysics Toolbox. Spat. Vis. *10*, 433–436.
57. Pelli, D.G. (1997). The VideoToolbox software for visual psychophysics: transforming numbers into movies. Spat. Vis. *10*, 437–442.
58. Peirce, J.W. (2007). PsychoPy–psychophysics software in Python. J. Neurosci. Methods *162*, 8–13.
59. Peirce, J.W. (2009). Generating stimuli for neuroscience using PsychoPy. Front. Neuroinform. *2*, 10.
60. Kuhn, M. (2008). Building predictive models in R using the caret package. J. Stat. Softw. *28*, 1–26.
61. Karatzoglou, A., Smola, A., Hornik, K., and Zeileis, A. (2004). kernlab - an S4 package for kernel methods in R. J. Stat. Softw. *11*, 1–20.
62. Kay, K.N., Winawer, J., Mezer, A., and Wandell, B.A. (2013). Compressive spatial summation in human visual cortex. J. Neurophysiol. *110*, 481–494.
63. Oosterhof, N.N., Connolly, A.C., and Haxby, J.V. (2016). CoSMoMVPA: multi-modal multivariate pattern analysis of neuroimaging data in Matlab/GNU Octave. Front. Neuroinform. *10*, 27.
64. Setsompop, K., Gagoski, B.A., Polimeni, J.R., Witzel, T., Wedeen, V.J., and Wald, L.L. (2012). Blipped-controlled aliasing in parallel imaging for simultaneous multislice echo planar imaging with reduced g-factor penalty. Magn. Reson. Med. *67*, 1210–1224.
65. Moeller, S., Yacoub, E., Olman, C.A., Auerbach, E., Strupp, J., Harel, N., and Uğurbil, K. (2010). Multiband multislice GE-EPI at 7 tesla, with 16-fold acceleration using partial parallel imaging with application to high spatial and temporal whole-brain fMRI. Magn. Reson. Med. *63*, 1144–1153.
66. Feinberg, D.A., Moeller, S., Smith, S.M., Auerbach, E., Ramanna, S., Gunther, M., Glasser, M.F., Miller, K.L., Ugurbil, K., and Yacoub, E. (2010). Multiplexed echo planar imaging for sub-second whole brain FMRI and fast diffusion imaging. PLoS ONE *5*, e15710.
67. Xu, J., Moeller, S., Auerbach, E.J., Strupp, J., Smith, S.M., Feinberg, D.A., Yacoub, E., and Uğurbil, K. (2013). Evaluation of slice accelerations using multiband echo planar imaging at 3 T. Neuroimage *83*, 991–1001.
68. Van Dijk, K.R.A., Hedden, T., Venkataraman, A., Evans, K.C., Lazar, S.W., and Buckner, R.L. (2010). Intrinsic functional connectivity as a tool for human connectomics: theory, properties, and optimization. J. Neurophysiol. *103*, 297–321.
69. Power, J.D., Barnes, K.A., Snyder, A.Z., Schlaggar, B.L., and Petersen, S.E. (2012). Spurious but systematic correlations in functional connectivity MRI networks arise from subject motion. Neuroimage *59*, 2142–2154.
70. Carp, J. (2013). Optimizing the order of operations for movement scrubbing: Comment on Power et al. Neuroimage *76*, 436–438.
71. Glasser, M.F., Sotiropoulos, S.N., Wilson, J.A., Coalson, T.S., Fischl, B., Andersson, J.L., Xu, J., Jbabdi, S., Webster, M., Polimeni, J.R., et al.; WU-Minn HCP Consortium (2013). The minimal preprocessing pipelines for the Human Connectome Project. Neuroimage *80*, 105–124.
72. Hastie, T., Friedman, J., and Tibshirani, R. (2009). The Elements of Statistical Learning, Second Edition (New York: Springer).
73. Varma, S., and Simon, R. (2006). Bias in error estimation when using cross-validation for model selection. BMC Bioinformatics *7*, 91.
74. Pereira, F., Mitchell, T., and Botvinick, M. (2009). Machine learning classifiers and fMRI: a tutorial overview. Neuroimage *45* (1, Suppl), S199–S209.
75. Haynes, J.D. (2015). A primer on pattern-based approaches to fMRI: principles, pitfalls, and perspectives. Neuron *87*, 257–270.
76. Golland, P., and Fischl, B. (2003). Permutation tests for classification: towards statistical significance in image-based studies. Inf. Process. Med. Imaging *18*, 330–341.
77. Etzel, J.A., and Braver, T.S. (2013). MVPA permutation schemes: permutation testing in the land of cross-validation, In 2013 International Workshop on Pattern Recognition in Neuroimaging (IEEE), pp. 140–143.
78. Etzel, J.A. (2015). MVPA permutation schemes: permutation testing for the group level, In 2015 International Workshop on Pattern Recognition in NeuroImaging (IEEE), pp. 65–68.
79. Phipson, B., and Smyth, G.K. (2010). Permutation p-values should never be zero: calculating exact p-values when permutations are randomly drawn. Stat. Appl. Genet. Mol. Biol. *9*, e39.
80. Mourão-Miranda, J., Bokde, A.L.W., Born, C., Hampel, H., and Stetter, M. (2005). Classifying brain states and determining the discriminating activation patterns: support vector machine on functional MRI data. Neuroimage *28*, 980–995.
81. Wang, Z., Childress, A.R., Wang, J., and Detre, J.A. (2007). Support vector machine learning-based fMRI data group analysis. Neuroimage *36*, 1139–1151.

82. Stelzer, J., Buschmann, T., Lohmann, G., Margulies, D.S., Trampel, R., and Turner, R. (2014). Prioritizing spatial accuracy in high-resolution fMRI data using multivariate feature weight mapping. Front. Neurosci. *8*, 66.

83. Smith, S.M., and Nichols, T.E. (2009). Threshold-free cluster enhancement: addressing problems of smoothing, threshold dependence and localisation in cluster inference. Neuroimage *44*, 83–98.

84. Nichols, T.E., and Holmes, A.P. (2002). Nonparametric permutation tests for functional neuroimaging: a primer with examples. Hum. Brain Mapp. *15*, 1–25.

85. Eklund, A., Nichols, T.E., and Knutsson, H. (2016). Cluster failure: why fMRI inferences for spatial extent have inflated false-positive rates. Proc. Natl. Acad. Sci. USA *113*, 7900–7905.

86. Drucker, H., Burges, C.J.C., Kaufman, L., Smola, A., and Vapnik, V. (1996). Support vector regression machines. In NIPS'96 Proceedings of the 9th International Conference on Neural Information Processing Systems, M.I. Jordan, and T. Petsche, eds. (MIT), pp. 155–161.

87. Nichols, T.E., Das, S., Eickhoff, S.B., Evans, A.C., Glatard, T., Hanke, M., Kriegeskorte, N., Milham, M.P., Poldrack, R.A., Poline, J.B., et al. (2017). Best practices in data analysis and sharing in neuroimaging using MRI. Nat. Neurosci. *20*, 299–303.

88. Boynton, G.M., Engel, S.A., Glover, G.H., and Heeger, D.J. (1996). Linear systems analysis of functional magnetic resonance imaging in human V1. J. Neurosci. *16*, 4207–4221.

89. Dumoulin, S.O., and Wandell, B.A. (2008). Population receptive field estimates in human visual cortex. Neuroimage *39*, 647–660.

STAR★METHODS

KEY RESOURCES TABLE

REAGENT or RESOURCE	SOURCE	IDENTIFIER
Software and Algorithms		
MATLAB	MathWorks, Natick, MA	http://www.mathworks.com/products/matlab/; RRID: SCR_001622
R	R Foundation for Statistical Computing, Vienna, Austria	http://www.r-project.org/; RRID: SCR_001905
FreeSurfer	[51]	http://surfer.nmr.mgh.harvard.edu/; RRID: SCR_001847
FSL	[52, 53]	http://www.fmrib.ox.ac.uk/fsl/; RRID: SCR_002823
SUIT Toolbox	[54, 55]	http://www.icn.ucl.ac.uk/motorcontrol/imaging/suit.htm; RRID: SCR_004969
Psychophysics Toolbox	[56, 57]	http://psychtoolbox.org/; RRID: SCR_002881
PsychoPy	[58, 59]	http://www.psychopy.org; RRID: SCR_006571
caret Package	[60]	http://topepo.github.io/caret/index.html
kernlab Package	[61]	https://cran.r-project.org/web/packages/kernlab/index.html
analyzePRF Toolbox	[62]	https://github.com/kendrickkay/analyzePRF
CoSMoMVPA Toolbox	[63]	http://cosmomvpa.org; RRID: SCR_014519

CONTACT FOR REAGENT AND RESOURCE SHARING

Further information and requests for resources and reagents should be directed to and will be fulfilled by the Lead Contact, David C. Somers (somers@bu.edu).

EXPERIMENTAL MODEL AND SUBJECT DETAILS

20 healthy subjects participated in this study. The Institutional Review Board of Boston University approved the study. All subjects were compensated and gave written informed consent to participate in the study. Subjects were recruited from Boston University and the Greater Boston area. All subjects were right-handed and had normal or corrected-to-normal vision. 10 subjects participated in experiment 1. Due to a large displacement in head position, functional data from a large portion of the cerebellum was irretrievably lost in one subject. As a result, this subject was removed from further analysis, leaving us with 9 subjects (3 female). Resting state data from an additional 5 subjects (5 female) were used in a subset of analyses. 5 subjects (3 female) participated in experiment 2. 3 subjects participated in both experiments. Subjects in experiment 1 ranged in age from 24 to 38 years, and subjects in experiment 2 ranged in age from 27 to 35 years. All subjects were screened for MRI contraindications prior to scanning.

METHOD DETAILS

Magnetic Resonance Image Acquisition

Experiment 1

Data were acquired from a 3 Tesla Siemens TIM Trio magnetic resonance imager located at the Center for Brain Science at Harvard University in Cambridge, Massachusetts. A 32-channel head coil was used for all scans. A high-resolution (1.0 × 1.0 × 1.3 mm) magnetization-prepared rapid gradient-echo (MPRAGE) sampling structure scan was acquired for each subject. The cerebral cortical surface of each hemisphere was then computationally reconstructed from this anatomical volume using Freesurfer software (version 5.3.0; http://surfer.nmr.mgh.harvard.edu/; [51]). T2*-weighted EPI (BOLD) images were acquired using a slice-accelerated EPI sequence that permits simultaneous multi-slice acquisitions using the blipped-CAIPI technique [TR = 2 s, TE = 30 ms; flip angle = 80°; 6/8 partial-fourier acquisition] [64]. A total of 69 slices were acquired with a slice acceleration factor of 3 and 0% skip, covering the whole brain, including the cerebellum. Images were acquired at a nominal 2mm isotropic spatial resolution (matrix size = 108 × 108 × 69).

Experiment 2

Data were acquired from a 3 Tesla Siemens Prisma scanner located at the Center for Brain Science at Harvard University in Cambridge, Massachussetts using a 64-channel head coil. High-resolution T1-weighted multiecho MPRAGE (Sagittal; TR = 2780 ms; TE = 1.32 ms, 3.19 ms, 5.11 ms, 7.03 ms; FA = 7°; 0.8 mm isotropic voxels; 224 slices; FOV = 256 mm × 256 mm × 180 mm; in-plane GRAPPA acceleration 2) and T2-weighted (Sagittal; TR = 3200 ms; TE = 564 ms; 0.8 mm isotropic voxels;

224 slices; FOV = 256 mm × 256 mm × 180 mm; in-plane GRAPPA acceleration 2) structural images were acquired. Functional data were acquired using a multi-band gradient-echo echo-planar pulse sequence [65–67] with the following acquisition parameters: TR = 650 ms; TE = 34.8 ms; FA = 52°; 2.3 mm isotropic voxels; FOV = 207 mm × 207 mm × 148 mm. A short TR was chosen in order to increase the number of time points recorded, as this was expected to enhance the quality of the pRF mapping. The increase in temporal sampling rate required a modest increase in voxel size relative to experiment 1. A total of 64 slices were acquired with a slice acceleration factor of 8 and 0% skip, fully covering the cerebral cortex and cerebellum. Spin echo field maps were also acquired with opposite phase encoding directions (Anterior-to-Posterior; Posterior-to-Anterior) and matching parameters to the gradient-echo EPI fMRI timeseries.

Magnetic Resonance Image Preprocessing

Experiment 1

Task and resting-state data were preprocessed using the Freesurfer FS-FAST software package (version 5.3.0) (Charlestown; http://surfer.nmr.mgh.harvard.edu/) [51]. The following preprocessing steps were performed: slice-time correction, motion-correction, and spatial normalization to a spatially unbiased infratentorial template (SUIT) of the human cerebellum and brainstem using a non-linear deformation [54, 55]. Data were then spatially smoothed with a 3 mm FWHM Gaussian kernel. Smoothing was constrained to only occur within cerebellar cortex as defined by the SUIT anatomical atlas [55]. Resting state data were then further preprocessed in MATLAB using custom scripts. We performed nuisance signal regression of head-motion (6 motion parameters and their 6 temporal derivatives), whole-brain signal, and ventricular and white matter signals [68]. We then calculated framewise displacement by taking the sum of the absolute derivatives of the 6 motion parameters for each time point [69]. A threshold of 0.5 mm was set to identify time points with excessive motion. To avoid artifact spread during bandpass filtering, high motion time points were replaced using linear interpolation [70]. Band-pass filtering was then performed (0.01–0.08 Hz). After filtering, high-motion time points were removed.

Experiment 2

Functional task data first underwent the Human Connectome Project's 'minimal' preprocessing pipeline, which comprises gradient nonlinearity distortion correction, motion correction, EPI image distortion correction, and co-registration with the subject's T1-weighted image [71]. The transforms involved in each step of this pipeline were concatenated into a single nonlinear transformation and performed as a single resampling step to reduce interpolation related blurring [71]. Following these preprocessing steps, functional images were further non-linearly transformed to the SUIT template [54, 55]. Data were then spatially smoothed within cerebellar cortex with a 3 mm FWHM Gaussian kernel.

Visual stimuli and experimental paradigm

Experiment 1 – VWM change detection paradigm

Stimuli were generated using the Psychophysics Toolbox extension [56, 57] in MATLAB (Mathworks, Natick, MA), and displayed using a liquid crystal display projector that back-projected onto a screen within the scanner bore. Subjects fixated on a centrally located crosshair, while 12 oriented colored bars were presented (six in each hemifield). While the number of presented bars in each hemifield was held constant across trials, the number of to-be-remembered items presented within a given block was either 1 or 4. The remaining bars in the display served as distractors. Target and distractors were distinguished by color, with targets shown in red and distractors shown in blue. Each bar subtended 0.25° x 2.5° of visual angle. The stimulus display subtended 25.6° x 19.2° of visual angle. Targets were limited to either the right or the left hemifield (counterbalanced across blocks). All bars in the display were randomly oriented at one of four possible angles (0°, 45°, 90°, 135°). Each subject completed 8 runs (total time per run = 6 min 16 s). Each fMRI task run contained 10 34 s task blocks and 16 s of blank fixation before and after the task blocks. Each block of trials consisted of a 2 s cue indicating the location of the target stimuli (left or right hemifield), followed by 8 4 s trials. On each VWM trial, a memory sample display was presented for 200 ms. Subjects were instructed to maintain the orientations of the presented target items over a 1000 ms delay period. After the sample and delay period, a memory probe was presented for 1800 ms. A 1000 ms fixation period separated each trial. On 50% of trials one of the target bars changed its orientation from the sample period to the probe period, while on the other 50% of trials no changed occurred. Subjects could respond during either the memory probe or the inter-trial fixation period by pressing a key to indicate that the orientation of the target had changed, or a separate key if it had not changed. The magnitude of the change on change trials was held constant at 90° (e.g., 0° to 90° or 45° to 135°). During sensorimotor control blocks, subjects were presented a display consisting entirely of distractors (all blue) and were instructed to press either key during the probe or inter-trial fixation period. Subjects also underwent 2-3 resting-state scans using identical scan parameters (each 180 TRs; 6 min duration). During the resting-state scans, subjects were instructed to let their minds wander while maintaining fixation on a centrally located crosshair.

Experiment 2 – Population receptive field mapping procedure

Stimuli were generated and presented using Python with the PsychoPy software package [58, 59]. The paradigm was adapted from the procedure described in [22]. Stimulus presentation was confined to a 16.2° × 16.2° field of view. The stimulus consisted of a bar aperture which subtended 16.2° in length and subtended either 1°, 2°, or 3° in width. The use of different bar widths can aid the estimation of pRF size. The width of the bar aperture was held constant within each run. Functional time-series of runs consisting of the same bar width were averaged prior to pRF modeling. The bar aperture comprised 3 equally sized rectangular patches of moving dots. Dot patches swept across the visual field in a discrete manner, changing location every 1.95 s (3 TRs). The step size of each change in location was 1.1 degrees. There were four possible sweep directions: left to right, right to left, top to bottom, and

bottom to top. Each sweep consisted of 13 steps/trials. A full sweep of the visual display was followed by a 9.75 s blank fixation interval (15 TRs). Each patch spanned 5.2° along the side perpendicular to the sweep direction. A 0.3° gap separated each patch. Patches of width 1°, 2°, and 3° contained 100, 200, and 300 dots, respectively. Dots moved at 1.5 deg/s and updated their position 60 times per second.

At each location, observers discriminated which of the two flanking patches contained dots moving in the same direction as the middle patch. Only one of the flanker patches moved in the same direction as the middle patch on each trial. Dot motion within the middle patch was always 100% coherent. Coherent dots moved along the length of the patch opposite to the sweep direction (left or right for vertical sweeps and up or down for horizontal sweeps). The coherence of the flanker patches' dot motion was staircased using a 1-up 3-down procedure. Moving dots had a limited lifetime of 10 frames (167 ms). Each noise dot moved in a random direction for the extent of its lifetime.

QUANTIFICATION AND STATISTICAL ANALYSIS

Multivariate pattern analysis

Patterns of cerebellar BOLD activity were obtained by temporally averaging the middle 9 TRs (18 s) of each VWM task block (34 s; set size 1 and 4 conditions) for each voxel in the cerebellum, thus ensuring independence of activity patterns between blocks. Support vector machines (SVM) were trained to discriminate the direction of attentional deployment using a leave-one-run-out cross-validation procedure. Analyses were performed in R 3.2.3 using the caret (version 6.0-68 [60];) and kernlab (version 0.9-25 [61];) packages. Classifier performance was assessed by predicting the class labels of each hold-out run. Classification accuracies were then averaged across hold-out sets to yield an overall accuracy for each ROI and subject. The cost parameter *C,* which is a regularization parameter that controls the bias-variance tradeoff [72], was tuned by performing an inner leave-one-run-out cross-validation loop on each training set. The search space of *C* ranged from 2^-2 to 2^4. Nested cross-validation schemes provide an unbiased method for selecting model hyperparameters [73–75]. Significance was evaluated using permutation tests [76]. To estimate a null distribution, a data-wise permutation scheme was employed in which class labels were permuted within-run prior to cross-validation [77]. This procedure was performed 1000 times. On each respective permutation, the same permutation scheme was used for each subject. A permuted group-level accuracy was computed by averaging individual subject accuracies [78]. We then compared our constructed null distribution to the decoding accuracy obtained with the true class labeling. A p value was computed as [(# of permutation accuracies $\geq$ true accuracy) + 1] / (N permutations + 1) [79].

Multivariate feature weight mapping

To finely localize spatially selective attentional responses within the cerebellum, we performed a multivariate feature weight mapping analysis on whole-cerebellum BOLD activity patterns [80–82]. The SVM algorithm defines a discriminant function that can be used to predict the class of new samples:

$$g(x) = wx + b.$$

where w is a vector of weights, x is a vector of voxel BOLD amplitude values, and b is a bias term. The weight vector (w) reflects the contribution of each voxel to the classification decision. By submitting whole-cerebellum multi-voxel activity patterns to the classification procedure, we obtained weights for every voxel in the cerebellum for each cross-validation fold. To reduce computation time on our computing cluster, PCA was used to orthogonally transform our original features (all cerebellar voxels) into principal components (# PCs = # samples – 1). The SVM classifier was then trained on this dimensionality-reduced matrix. The resulting principal component weight vector could then be transformed back to the original feature space by reversing the PCA transformation (e.g., [80–82]), thus resulting in a weight for each feature (voxel). Final weights were computed by averaging weights across cross-validation folds. We then generated an empirical null distribution of weights for each voxel in the cerebellum by training the whole-cerebellum classifier 1000 times with permuted class labels. We could then assess the discriminative value of a voxel by computing the probability of obtaining a weight that is at least as extreme as the observed weight given the voxel's null weight distribution. Probabilities were computed for all cerebellar voxels in the original weight map as well for each permuted weight map. Each voxel probability was then subtracted from 1 to generate a cumulative probability and then converted to a *z*-score using MATLAB's *norminv* function. To maintain information about the direction of discriminance, voxel *z*-scores were signed according to the direction of the effect (left or right tail of null distribution). Actual discriminance *z*-maps and permuted *z*-maps were then submitted to a 2nd-level group analysis. To control family-wise error rate, we employed threshold-free cluster enhancement (TFCE) [83] and non-parametric randomization tests [84]. First, group statistic maps were generated via voxel-wise t tests with variance smoothing (σ = 4 mm) followed by TFCE transformation as implemented by FSL's *randomise* tool (http://www.fmrib.ox.ac.uk/fsl/randomise; [52, 53]). A null distribution was then generated by recording the image-wise maximum TFCE statistic for each permuted group map [84, 85]. Using this maximum statistic null distribution, the original group map was thresholded at $p < 0.05$, two-sided. In order to compare our cerebellar results with regions with well-documented spatial selectivity in the cerebral cortex, we additionally performed feature weight mapping on whole-cortex activity patterns. As FSL's *randomize* tool is not compatible with Freesurfer functional surface files, we used the CoSMoMVPA analysis package's surface-based implementation of TFCE [63].

Eye movement control analysis

As the cerebellum has previously been implicated in eye movements, subjects were instructed to maintain fixation on a centrally located cross while performing the task using covert attention. All subjects were experienced visual psychophysical observers. Additionally, subjects practiced holding central fixation while performing the task prior to scanning. During scanning, eye position was monitored using an EyeLink 1000 from SR research. Eye tracking data could not be obtained for one of our subjects in Experiment 1 due to technical difficulties. To examine the relationship between any residual eye movements and cerebellar activation, we used linear support vector regression (SVR) ($\varepsilon = 0.1$) [86] to predict a continuous measure of eye movements from the pattern of BOLD activity extracted from a cerebellar ROI. Our cerebellar ROI included any cerebellar voxel that was considered significant at the group level of the multivariate feature weight mapping analysis ($p < 0.05$ FWE corrected, two-sided). Model performance assessment and hyperparameter tuning were carried out using the same nested cross-validation procedure described previously. For each trial within a block, we quantified the magnitude of eye movement by computing the root mean square deviation from the median gaze position for the trial. We also computed the average horizontal gaze position for each trial. These values were averaged across trials to generate a mean value for each block. Some blocks had missing eye position data as a result of the eye tracker being unable to locate the subject's pupil (excessive eye blinks or interference from eye lids). Consequently, for some subjects training or test sets contained different number of samples across different cross-validation folds. The accuracy of SVR predictions was assessed by computing a cross-validated coefficient of determination or R^2.

$$R^2_{cv} = 1 - \frac{\sum_{i=1}^{n_{test}} (y_i - \hat{y}_i)^2}{\sum_{i=1}^{n_{test}} (y_i - \bar{y}_{train})^2}$$

where $\hat{y}_i$ denotes the SVR prediction for the i^{th} test set observation and $\bar{y}_{train}$ indicates the response mean of the training set. In cases where explained variance is very low, R^2_{cv} can be negative [87]. Negative values of R^2_{cv} indicate that the fitted model performs worse than a null model in which the response of each test set observation is predicted to be the mean response of the training set.

VWM load/spatial coding selectivity analysis

Cortico-cerebellar VWM load activation was identified by fitting a voxel-wise general linear model that included a predictor for each task condition. Model fitting was performed using the Freesurfer FS-FAST software package (version 5.3.0) (Charlestown; http://surfer.nmr.mgh.harvard.edu/) [51]. To control for activation due to cue reorientation, cue time points at the beginning of each block were included as nuisance regressors in the model. Singular value decomposition reduced the 6 motion correction vectors obtained during preprocessing to 3 eigenvectors, which were also included as nuisance regressors in the model. Task regressors were convolved with a canonical hemodynamic response function prior to fitting. The hemodynamic response was modeled by a γ function with a delay of $\delta = 2.25$ s and a decay time constant of $\tau = 1.25$ [88]. t tests were performed voxel-wise, contrasting the set size 4 condition with the set size 1 condition. Individual subject *t*-statistic maps were then submitted to 2nd-level group analysis. Mirroring the feature weight group analysis, voxel-wise t tests were performed with variance smoothing ($\sigma = 4$ mm). The resulting *t*-statistic map then underwent TFCE transformation [83]. To correct for multiple comparisons, the maximal test statistic was retained for all possible permutations or sign-flips ($n = 512$) [84, 85]. Using this null distribution, the group VWM load map was thresholded at $p < 0.05$, one-sided.

To assess the relative strength of load activation and spatial selectivity within the cerebellum and cerebral cortex, uncorrected group *t*-statistic maps from spatial and load analyses were normalized across either the cerebellum or cerebral cortex. Prior to normalization, we took the absolute value of the spatial *t* map, as both extremes of the distribution indicate spatial selectivity. We then directly contrasted the normalized VWM load activation map and normalized spatial coding discriminance map via subtraction. After taking the difference of the two maps, any voxel/vertex that did not survive correction for multiple comparisons in both analyses was masked out.

A similar procedure was performed on resting-state correlation maps to contrast the connectivity of spatial and load sensitive portions of the ventral cerebellum. Resting-state data collected across 18 sessions and 14 subjects (4 subjects scanned twice) were included in this analysis. Spatial- and load-selective seed ROIs were defined in each hemisphere of lobule VIIb/VIIIa by the intersection of a hemispheric lobule VIIb/VIIIa anatomical mask and the multiple comparison corrected group map of each analysis. Mean time courses extracted from these ROIs were then correlated with every vertex from the contralateral hemisphere of cerebral cortex. Cerebral cortical correlation maps were normalized using Fisher's *z* transformation. For subjects with multiple sessions, *z* maps were averaged prior to the 2nd-level group analysis. We then performed the same procedure previously carried out on the spatial and load selectivity group maps (normalization, subtraction, and masking). To assess the relationship between task selectivity and cortico-cerebellar connectivity we computed the spatial correlation between the task difference map and the connectivity difference map.

Population receptive field modeling

pRF analysis was performed using the analyzePRF MATLAB toolbox [62]. Voxel time-series were modeled with a compressive summation model [62], which is an extension of the pRF model described by [89]. This model includes an additional exponent parameter to account for subadditive spatial summation [62]. The model is formally expressed as:

$$r(t) = g \times \left[\int S(x,y)\, G(x,y)\, dxdy \right]^n$$

where $r(t)$ is a voxel's predicted response, g is a gain parameter, S is a binary stimulus mask, and G is a 2-dimensional isotropic Gaussian expressed as:

$$G(x,y) = e^{-\frac{(x-x_0)^2+(y-y_0)^2}{2\sigma^2}}$$

where x_0 and y_0 are parameters defining the position of the Gaussian, and σ is a parameter defining the standard deviation of the Gaussian. Prior to fitting, functional time-series of runs consisting of the same experimental bar size (1, 2 or 3°) were averaged. The original pRF model described by [89] involved a two-stage fitting procedure: an initial coarse grid-fit followed by an exhaustive non-linear optimization procedure using seed parameters from the grid-fit. However, a recent study found that the full optimization procedure did not outperform the coarse grid-fit when predicting independent, left-out data [22]. It was argued that the grid-fit procedure is more robust to noise and better able to predict the responses of fronto-parietal voxels with large pRFs [22]. As cerebellar lobule VIIb/VIIIa possesses similar profiles of connectivity and task recruitment as fronto-parietal regions, we only performed the initial grid-fit procedure. This analysis was restricted to the ventral cerebellum. The grid-fitting procedure iterated over 7720 possible parameter combinations (16 angles, 13 eccentricities, 8 widths, and 5 exponents). A 3-fold cross-validation procedure was used to determine which voxels were further analyzed. Each fold included all three experimental bar sizes. We excluded voxels that did not exceed a cross-validated predicted-actual correlation of 0.2.

DATA AND SOFTWARE AVAILABILITY

All data and code used for data analysis are available upon request to the authors.